ARTICLE

Check for updates

Stripe skyrmions and skyrmion crystals

X. R. Wang [1,2 ✉], X. C. Hu[1,2] & H. T. Wu[1,2]

Skyrmions are important in quantum field theory and information technology for being topological solitons and for their attractive applications. Magnetic skyrmions are believed to be circular and stripy spin textures accompanied skyrmion crystals (SkXs) termed spiral/helical/cycloid orders have zero skyrmion number. Here we show that those stripy spin textures are skyrmions, siblings of circular skyrmions in SkXs and cousins of isolated circular skyrmions. Various irregular morphologies are the nature structures of skyrmions in the ground states. At the extreme of one skyrmion in the whole sample, the skyrmion is a ramified stripe. As the skyrmion number density increases, skyrmion shapes gradually change from ramified stripes to rectangular stripes, and eventually to circular objects. At a high skyrmion number density, SkXs are the preferred states. Our findings reveal the nature and properties of stripy spin texture, and open an avenue for manipulating skyrmions.

[1] Physics Department, The Hong Kong University of Science and Technology, Clear Water Bay, Kowloon, Hong Kong, P.R. China. [2] HKUST Shenzhen Research Institute, Shenzhen 518057, China. ✉email: phxwan@ust.hk

Skyrmions, originally for resonance states of baryons[1], were first unambiguously observed in the form of skyrmion crystals (SkXs) in various chiral magnets and by various experimental techniques[2–7]. Magnetic skyrmions are topological non-trivial spin textures of magnetic films characterized by a skyrmion number of $Q = \frac{1}{4\pi} \int \mathbf{m} \cdot (\partial_x \mathbf{m} \times \partial_y \mathbf{m}) \, \mathrm{d}x\mathrm{d}y$, here $\mathbf{m}$ is the unit vector of magnetization. Q must be an integer for an infinite magnetic film, and a non-zero Q spin texture is called a skyrmion of skyrmion number Q. It was isolated circular skyrmions, not an SkX, that were predicted in early theories[8,9]. Isolated skyrmions were indeed observed later in confined structures and films[10–15]. It is an experimental fact that SkXs form in a very narrow magnetic-field-temperature window. Outside the window, stripy phases appear. Stripes, which can even coexist with SkXs, are in fact easier to form than an SkX does. In contrast, those stripy phases do not appear together with isolated skyrmions. Interestingly, stripes were observed many years before the SkXs[16]. These stripy phases are called helical, spiral, and cycloid spin orders. A one-dimensional model[9,17–21] was used to describe the rotation of spins perpendicular to stripes. To date, a holistic description of various stripy structures, especially ramified stripes and stripy maze[22–29], is lacking. The general belief is that those stripes are not skyrmions and have zero skyrmion numbers[30] although some race-track stripes are called merons with 1/2 skyrmion number or bimerons[27,31,32].

In this article, we show that stripy magnetic textures appear in a chiral magnetic film with Dzyaloshinskii–Moriya interaction (DMI) are actually irregular skyrmions. Each stripy texture has exactly skyrmion number 1. The irregular shape is due to the negative skyrmion formation energy (relative to ferromagnetic state) when the ferromagnetic state is not the ground state. For a given system, the morphology of these skyrmions is random when the skyrmion number density is low. At extremely low density, magnetic textures are ramified stripes in order to maximize the negative skyrmion formation energy gain. The exact appearance of each pattern is very sensitive to the initial spin configuration and its dynamical path. The basic building blocks of irregular random skyrmions are stripes of well-defined width. The optimal width comes from the competition between Heisenberg's exchange energy and the DMI energy that, respectively, prefer a larger and smaller width. Unexpectedly, this exchange energy and DMI energy dependence of width are opposite to the skyrmion size of an isolated skyrmion that increases with DMI interaction and decreases with exchange energy[33,34].

Results

Model. We consider an ultra-thin ferromagnetic film of thickness d in the xy plane. The film has an exchange energy E_{ex} with exchange stiffness constant A, an interfacial DMI energy E_{DM} with DMI coefficient D, an anisotropy energy E_{an} with a perpendicular easy-axis anisotropy K, and the Zeeman energy E_{Ze} in a perpendicular magnetic field H. The total energy E_{total} reads

$$E_{total} = E_{ex} + E_{DM} + E_{an} + E_{Ze}, \quad (1)$$

where $E_{ex} = Ad \iint |\nabla \mathbf{m}|^2 \, \mathrm{d}S$, $E_{DM} = Dd \iint [m_z \nabla \cdot \mathbf{m} - (\mathbf{m} \cdot \nabla)m_z] \, \mathrm{d}S$, $E_{an} = Kd \iint (1 - m_z^2) \, \mathrm{d}S$, and $E_{Ze} = \mu_0 H M_s d \iint (1 - m_z) \, \mathrm{d}S$. M_s is the saturation magnetization and μ_0 is the vacuum permeability. The integration is over the whole film. The energy is set to zero, $E_{total} = 0$, for the ferromagnetic state of $m_z = 1$. $\mathbf{m}$ is assumed uniform in the thickness direction. The demagnetization effect is included in E_{an} through the effective anisotropy $K = K_u - \mu_0 M_s^2 / 2$ corrected by the shape anisotropy, here K_u is the perpendicular magnetocrystalline anisotropy. This is a good approximation when the film thickness d is much smaller than the exchange length[34]. It is known that isolated circular

skyrmions are metastable state of energy $8\pi A d\sqrt{1 - \kappa}$ when $\kappa = \pi^2 D^2/(16 AK) < 1$[34]. Here we use MuMax3 simulator[35] to numerically solve the Landau–Lifshitz–Gilbert (LLG) equation for the stable states in the opposite regime of $\kappa > 1$ where circular skyrmions are not stable states[34], see Method.

Ramified stripy skyrmions. For a sample of 300 nm × 300 nm × 0.4 nm under the periodical boundary conditions and with $A = 10$ pJ m^{-1}, $D = 6$ mJ m^{-2}, $K = 0.49$ MJ m^{-3}, and $M_s = 0.58$ MA m^{-1} that are typical values for those chiral magnets supporting SkXs[30,36,37], $\kappa > 1$, so that single domain and isolated circular skyrmion are not stable any more[34]. We will start from a small nucleation magnetic domain with sharp domain wall to speed up skyrmion formation dynamics although stripe skyrmions will appear spontaneously due to thermal or other fluctuations in reality. Figure 1 shows how a disk domain of diameter 20 nm (Fig. 1a), a hexagonal domain of side length 10 nm (Fig. 1b), and a square domain of length 20 nm (Fig. 1c) evolve according to the LLG equation with $\alpha = 0.25$. α will not change physics described below because we are interested in the spin textures of the LLG equation that do not vary with time. However, α can change the evolution path and energy dissipation rate so that it can influence which fixed point to pick when a system has many fixed points (different spin textures) like the current situation. This is similar to the sensitiveness of attractor basins to the damping in a macro spin system[38]. The initial configurations in Fig. 1a–c are obtained by reversing spins in the white regions from $m_z = -1$ to $m_z = 1$ such that the configurations have very sharp domain walls and zero skyrmion number $Q = 0$. Figure 1d–f and Fig. 1g–i show, respectively, the intermediate spin structures and final stable spin textures from the three different initial configurations of Fig. 1a–c. After a short time of order of picoseconds, the initial states transform into irregular structures of skyrmion number $Q = 1$, no matter whether the initial shape is circular or non-circular as shown in Fig. 1j–l where the time is in logarithmic scale. As time goes on, Q (the blue lines in Fig. 1j–l) stays at 1, and system energy E_{total} (the red curves) is negative and keeps decreasing until it reaches a stable ramified stripy spin texture. Clearly, this irregular ramified spin texture is a non-circular skyrmion whose formation energy is negative. The negative formation energy explains why the skyrmion prefers to stretch out to occupy the whole space to lower its energy. This process is clearly demonstrated in Supplementary Video 1 that shows how the system evolves from Fig. 1a to 1g and how Q grows from 0 to 1. The simulations show also that the exact pattern is very sensitive to the initial configuration and dynamical/kinetic paths as well as how energy dissipates. In a real system, the process shall proceed spontaneously from any randomly generated nucleation centre no matter by a thermal fluctuation or an intentional agitation.

We use color to encode the skyrmion charge density ρ defined as $\rho = \mathbf{m} \cdot (\partial_x \mathbf{m} \times \partial_y \mathbf{m})/(4\pi)$ as indicated by the color bar in Fig. 1. Interestingly, ρ is non-zero only around convex (positive) and concave (negative) areas. ρ is almost zero along the long straight stripe. This may explain why the skyrmion number of stripy textures was thought to be zero in the literature[30]. As shown in Fig. 1j–l, the sum of all positive and negative skyrmion charge is always quantized to 1 protected by the topology. The continuous decrease of energy E_{total} also indicates the final morphology of the ramified stripe skyrmions is not unique and depends on the dynamical path of the system evolution that in turn relates to the initial configuration.

Optimal stripe width. One striking feature about the stripes shown in Fig. 1 is a well-defined stripe width that is usually referred to a given wave vector in experiments. The competition between the exchange energy and DMI energy can easily lead to a A/D dependence[9,17–20]. However, it is highly non-trivial to
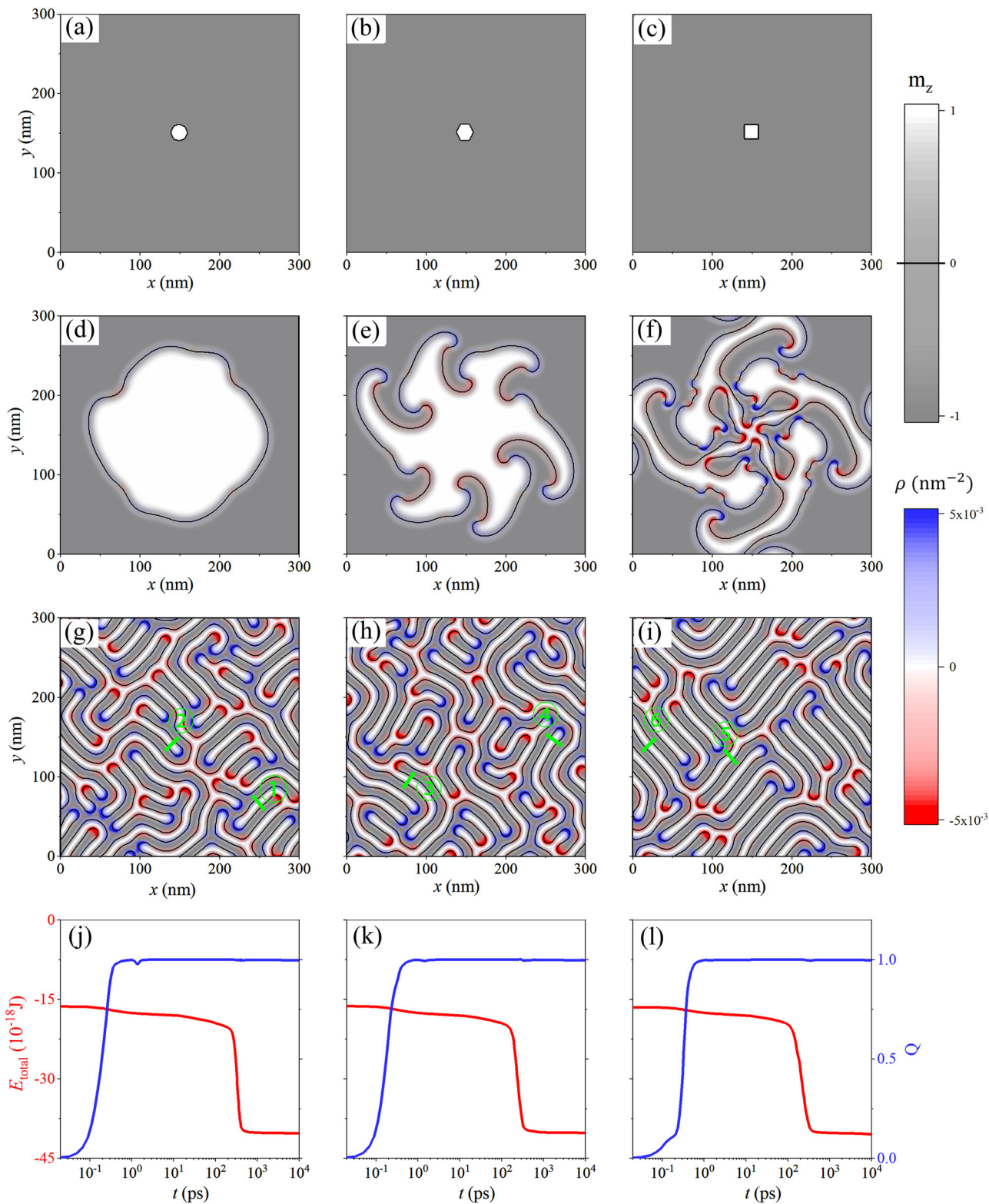
Fig. 1 Dependence of ramified stripe-morphology on nucleation domains. Numerical solutions of the Landau–Lifshitz–Gilbert equation with the periodical boundary conditions and $A = 10 \, \text{pJ m}^{-1}$, $D = 6 \, \text{mJ m}^{-2}$, $K = 0.49 \, \text{MJ m}^{-3}$, $M_s = 0.58 \, \text{MA m}^{-1}$ for a sample of 300 nm × 300 nm × 0.4 nm. A, D, K, and M_s are exchange stiffness constant, the Dzyaloshinskii–Moriya interaction coefficient, easy-axis anisotropy, and saturation magnetization, respectively. **a–c** are different initial configurations of a disk of diameter 20 nm (**a**), a hexagon of side length 10 nm (**b**) and a square of length 20 nm (**c**). **d–f** are intermediate states at 0.3 ns with irregular shapes. **g–i** are the final stable patterns with irregular ramified stripes. Skyrmion charge density ρ is encoded by colours (the blue for positive and the red for negative) while the grayscale encodes m_z. The dark black lines denote $m_z = 0$. The positive and negative charges exist respectively only around convex and concave areas. The spin profile across the stripes at the green ⊕ is considered. **j–l** are the evolution of total energy E_{total} and topological skyrmion number Q (t is in the logarithmic scale). Q reaches the skyrmion number 1 within 1 ps. Clearly, the skyrmion number is a constant and the total energy is negative and approaches a constant almost independent from the initial configurations.
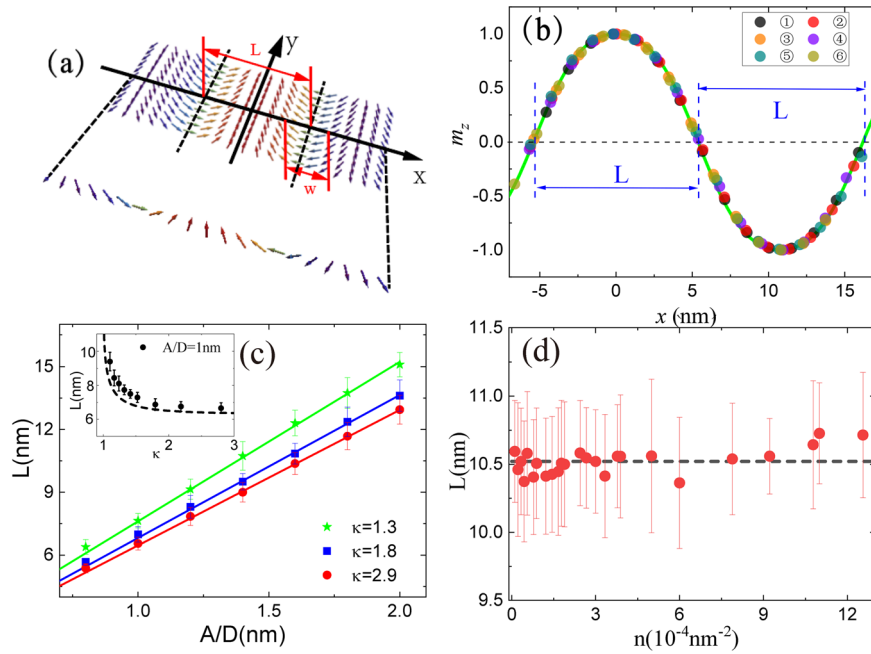
Fig. 2 Properties of stripe skyrmions. a Schematic diagram of spin texture of parallel stripes. **b** Symbols, from different stripes labelled by textcircledn in Fig. 1g–i, are $m_z = \cos\Theta$ from MuMax3. The green solid line is the fit of $\Theta(x) = 2\arctan\left[\frac{\sinh(|x|/w)}{\sinh(L/2w)}\right]$. ($\Theta \leq \pi/2$) and $\Theta(x) = 2\arctan\left[\frac{\sinh(L/2w)}{\sinh((|x|-L))/w)}\right]$ ($\Theta \geq \pi/2$) with $L = 10.78$ nm and $w = 3.05$ nm. $x = 0$ is the centres of white stripes. All data from different stripes fall onto the same curve means that stripes of the same width are basic building blocks of stripe skyrmions. **c** A/D-dependence of stripe width L for various $\kappa = \pi^2 D^2/(16AK) = 1.3$ (the green stars); 1.8 (the blue squares); and 2.9 (the red circles). The solid lines are the fits of $L = aA/D$ with $a = 7.61$ for $\kappa = 1.3$; $a = 6.82$ for $\kappa = 1.8$; $a = 6.47$ for $\kappa = 2.9$. Inset: the dependence of L on κ for $A/D = 1$ nm. A, D, and K are exchange stiffness constant, the Dzyaloshinskii–Moriya interaction coefficient, and easy-axis anisotropy, respectively. Symbols are the numerical data and the dashed line is the theoretical prediction without any fitting parameter. The error bar is the standard deviation of stripe width from various places. **d** The dependences of stripe width L on skyrmion number density for $A = 10$ pJ m^{-1}, $D = 6$ mJ m^{-2}, $K = 0.49$ MJ m^{-3}, and $M_s = 0.58$ MA m^{-1}. M_s is saturation magnetization. The number of skyrmions varies from 1 to 113 in our sample of 300 nm × 300 nm × 0.4 nm under the periodical boundary conditions. The dashed line is $L = 10.52$ nm. The error bars are the standard deviation of stripe width from various places.

understand the effect of the magnetic anisotropy on stripe width. In order to understand the underlying physics of this well-defined width, one needs a good spin texture profile along the direction perpendicular (x) to the stripes. We found that black ($m_z \leq 0$) and white ($m_z \geq 0$) stripes can be approximated by $\Theta(x) = 2\arctan\left[\frac{\sinh(L/2w)}{\sinh(|x|/w)}\right]$ and $\Theta(x) = 2\arctan\left[\frac{\sinh(|x|/w)}{\sinh(L/2w)}\right]$ ($|x| \leq L/2$), respectively. Θ is the polar angle of the magnetization at position x and $x = 0$ is the centre of a stripe. L and w measure respectively the stripe width and skyrmion wall thickness as schematically illustrated in Fig. 2a. Figure 2b demonstrates the excellence of this approximate profile for a set of model parameters of $A = 10$ pJ m^{-1}, $D = 6$ mJ m^{-2}, $K = 0.49$ MJ m^{-3}, and $M_s = 0.58$ MA m^{-1}. The y-axis is m_z and $x = 0$ is the stripe centre where $m_z = 1$. Different symbols are numerical data across different stripes labelled by the green ⊙ in Fig. 1g–i. The solid curve is the fit of profile $\cos\Theta(x)$ with $L = 10.78$ nm and $w = 3.05$ nm. All data from different stripes falling onto the same curve demonstrates that stripes, building blocks of pattern, are identical.

Using the excellent spin profile, one can obtain magnetic energy of a film filled with the stripe skyrmions as a function of L and w. Minimizing the energy against L and w allows us to obtain A, D, and K dependence of stripe width L and skyrmion wall thickness w. In terms of L, $\epsilon = L/(2w)$, $\xi = A/D$, and κ, the total system energy density of a film filled by such stripes is

$$E = \frac{4D}{\xi}\left[\frac{\xi^2}{L^2}g_1(\epsilon) - \frac{\pi\xi}{4L} + \frac{\pi^2}{64\kappa}g_2(\epsilon)\right], \qquad (2)$$

where $g_1(\epsilon) = \int_0^1 \frac{[2\epsilon\sinh(\epsilon)\cosh(\epsilon x)]^2}{[\sinh^2(\epsilon)+\cosh^2(\epsilon x)]^2}dx$, and $g_2(\epsilon) = \int_0^1 \frac{[2\sinh(\epsilon)\sinh(\epsilon x)]^2}{[\sinh^2(\epsilon)+\cosh^2(\epsilon x)]^2}dx$. The optimal stripe width obtained from minimizing energy E is $L = a\frac{4A}{\pi D}$, where a depends weakly on $\kappa = \pi^2 D^2/(16AK) > 1$. The physics of this result is clear: DMI energy is negative, and one can add more stripes by reducing L such that the total energy will be lowered. On the other hand, the exchange energy will increase with the decrease of L. As a result, L is proportional to A/D which is opposite to the behaviour of size of an isolated skyrmion whose size increases with D and decreases with A[30,34]. These theoretical results agree very well with micro-magnetic simulations as shown in Fig. 2c with $a = 7.61$ for $\kappa = 1.3$; $a = 6.82$ for $\kappa = 1.8$; $a = 6.47$ for $\kappa = 2.9$. The dependence of L on κ for a fixed $A/D = 1$ nm is shown in the inset. One can see that L depends weakly on large $\kappa \gg 1$. Unexpectedly, L are the same no matter whether we have one, two, or more ramified and non-ramified stripe skyrmions. This is reflected in the skyrmion number density independence of L as shown in Fig. 2d.

Transformation from stripy states to SkXs. To understand why condensed stripe skyrmions and SkXs can appear together in a given chiral magnetic film when the material parameters are fixed, we try to increase the number of skyrmions in our film of 300 nm × 300 nm × 0.4 nm. Encouraged by the results in Fig. 1 that each nucleation domain creates one irregular stripe skyrmion, we place 2, 100, and 169 small disk domains of diameter 10 nm as shown in Fig. 3a–c and let them evolve according to the LLG equation. Figure 3d–f are the final steady states. As expected, we indeed obtained two irregular ramified stripe skyrmions Fig. 3d. For the case of 100 skyrmions, some of them have
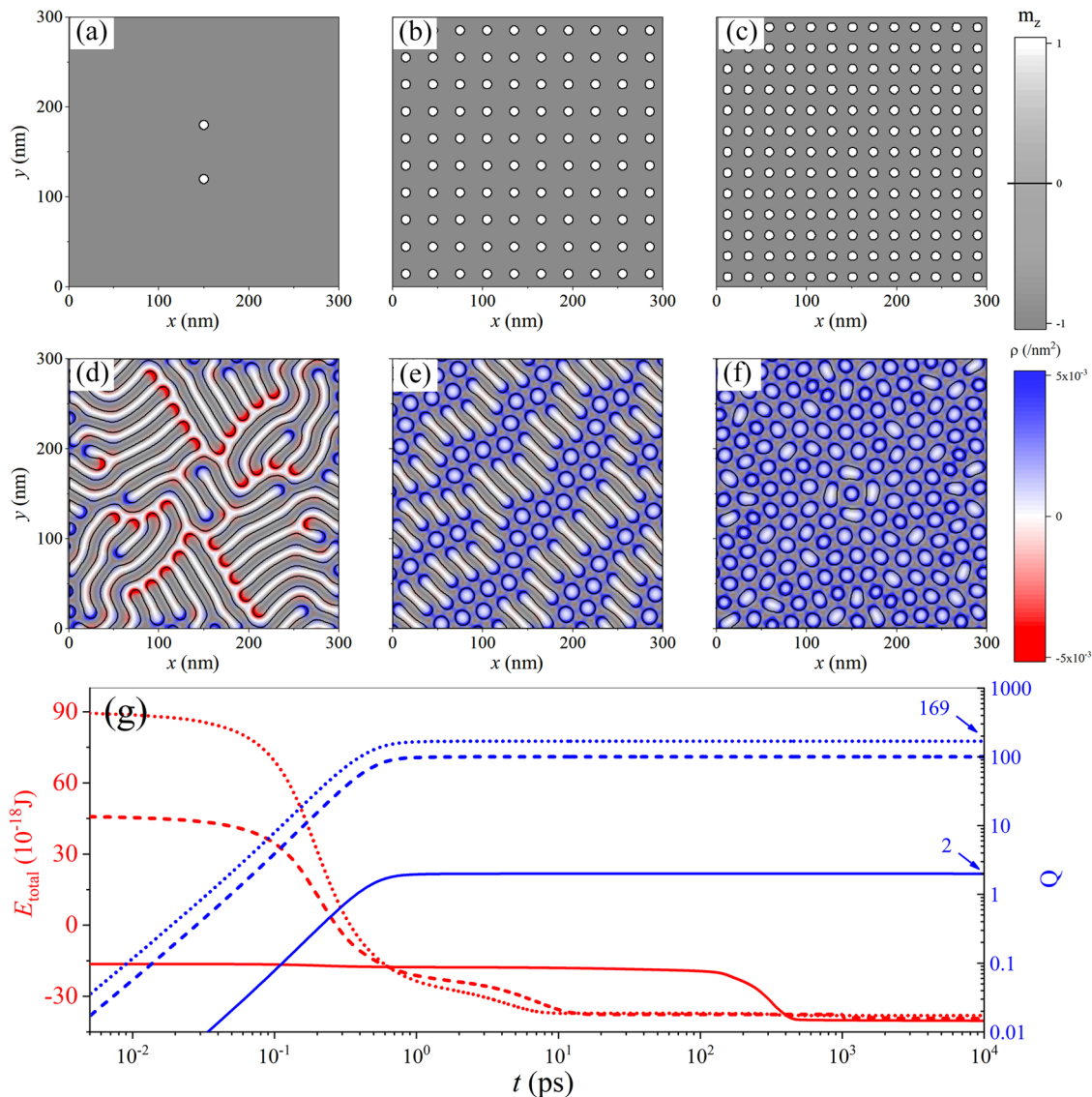
Fig. 3 Morphology change with skyrmion-number-density. Various number of skyrmions are created in a sample of 300 nm × 300 nm × 0.4 nm with the periodical boundary conditions from various nucleation domains in square lattice initially. The material parameters are the same as those in Fig. 1. The grayscale denotes the z-component of magnetization m_z. The topological charge density distributions in **a–f** are encoded in the color denoted by color bar of ρ (nm^{-2}). To speed up the system reaching its final stable states, we use a large Gilbert damping constant of $\alpha = 1$. **a–c** are the initial configurations with $N = 2$ (**a**), 100 (**b**) and 169 (**c**) nucleation domains, respectively. **d–f** are the final stable pattern. Skyrmion charge density ρ is encoded in colours (the red and the blue for positive and negative ρ respectively) while m_z is encoded in the grayscale. The dark black lines denote $m_z = 0$. The positive and negative charges exist respectively only around canvex and concave areas. **g** is the evolution of total energy E_{total} (the left y-axis) and topological skyrmion number Q (both Q and t are in the logarithmic scale). Clearly, Q reaches 2, 100, and 169, respectively, in a very short time. The total energy is negative and approaches a constant, indicating a stable state.

rectangular shape and are arranged in a nematic phase while the rest of skyrmions look like disks and are in a lattice structure Fig. 3e. In the case of 169 skyrmions, skyrmions are circular and are in a triangular lattice Fig. 3f. The skyrmion nature of the spin textures can be clearly confirmed by the change of Q (blue) with time as shown in Fig. 3g (the solid, dashed, and dotted lines for Q = 2, 100, and 169 respectively). Figure 3g shows also how system energy (the red lines) changes with time. One interesting feature is that total energy is not sensitive to skyrmion number density before skyrmion–skyrmion distance is comparable to the optimal stripe width and skyrmions take stripe shape. The system energy starts to increase with the skyrmion number density, and condensed skyrmions transform from rectangular stripe skyrmions in the nematic phase into circular skyrmions in a triangular lattice.

This feature does not favour SkX formation, and may explain why SkXs were observed in the presence of an external magnetic field: With only one skyrmion in the whole system as those shown in Fig. 1, the net magnetic moment is zero because spin up (white area) and down spin (black area) are almost equal so that magnetic moment cancel each other. As skyrmion number increases, the net magnetic moment increases and becomes non-zero.

Discussion
We have showed that stripe and ramified stripe skyrmions are essentially the same as the circular skyrmions in SkXs. The difference in skyrmion shapes at different skyrmion number density come from the skyrmion–skyrmion interaction. When the average
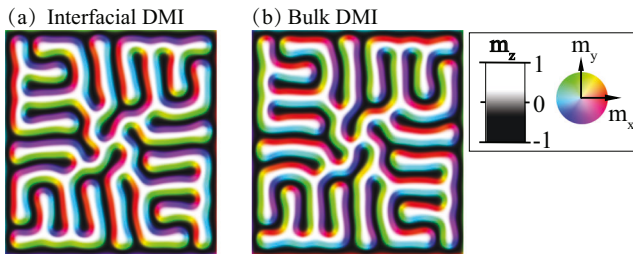
Fig. 4 Similarity of ramified stripe skyrmions in bulk and interfacial Dzyaloshinskii–Moriya interaction (DMI). Structures of one stripe skyrmion for interfacial (**a**) and bulk (**b**) DMIs starting from the same initial configurations. The sample size is 300 nm × 300 nm × 0.4 nm with the same model parameters as those for Fig. 1 except DMI coefficient $D =$ 4 mJ m^{-2}. The periodical boundary conditions are used in the simulations. The z-component of magnetization m_z is encoded in grayscale shown in the left color bar. The in-plane spin component is encoded by the colors denoted by the right color bar.

distance between two nearby skyrmions is order of the stripe width, the skyrmion–skyrmion repulsion compress skyrmions into circular objects. This understanding permits an SkX in the absence of an external magnetic field as long as one can use other means to add more skyrmions into a film such as a scanning tunnelling tip[6].

We have presented results for the interfacial DMI so far, similar results are also true for bulk DMI. As shown in Fig. 4, one ramified stripe skyrmion has very similar structures for interfacial Fig. 4a and bulk Fig. 4b DMIs when we start from the same initial configuration with the same interaction strength. The only difference is the change of Neel type of stripe wall to the Bloch-type stripe wall as shown by the color-coding in the figures.

A perpendicular magnetic field can modify the morphology and width of a stripe without changing its skyrmion number. Stripe width increases (decreases) with the field when out-of-plane spin component is anti-parallel (parallel) to the field.

It requires a certain amount of energy to destroy a stable or metastable state by definition. Thus, all skyrmions discussed in this paper are stable against thermal noise as long as the thermal energy is smaller than their potential barriers. Supplementary Video 2 shows the state in Fig. 3e stable at 50 K.

Skyrmions provide a fertile ground for studying fundamental physics. For example, the topological Hall effect is a phenomenon about how non-collinear magnetization in SkXs affects electron transport. Knowing stripy phases are also condensed irregular skyrmions, it expands surely arena of the topological Hall effect. We can not only study how electron transport be affected by the skyrmion crystals, but also skyrmions in other condensed phases such as nematic phases, or how the elongation and orientation of stripe skyrmion affect Hall transport. The discovery of stripe skyrmions allows us to investigate how the topology, the local and global geometries affect spin excitations separately.

The assertion that ramified stripes and other stripes appeared together with SkXs are irregular skyrmions are firmly confirmed by the nano-magnetic simulations. These stripes have a well-defined width that is from the competition between exchange interaction energy and DMI energy. The inverse of the width is the well-known wave vector used to describe the spiral spin order in the literature[16]. In contrast to isolated skyrmions whose size increases with DMI constant and decreases with the exchange stiffness constant, the stripe width increases with the exchange stiffness constant and decreases with the DMI constant. Counter-intuitively, SkXs are highly compressible like a gas, not like an atomic crystal. This detailed property need a careful further study. Our findings should have far reaching implications to skyrmion physics and to skyrmion-based applications.

Methods

Numerical simulations. Spin dynamics is governed by the LLG equation,

$$\frac{\partial \mathbf{m}}{\partial t} = -\gamma \mathbf{m} \times \mathbf{H}_{\text{eff}} + \alpha \mathbf{m} \times \frac{\partial \mathbf{m}}{\partial t}, \tag{3}$$

where $\mathbf{m}$, γ, α are respectively the unit vector of the magnetization, gyromagnetic ratio, and the Gilbert damping. $\mathbf{H}_{\text{eff}} = 2A\nabla^2\mathbf{m} + 2Km_z\hat{z} + \mathbf{H}_d + \mathbf{H}_{\text{DM}}$ is the effective field including the exchange field characterized by the exchange stiffness A, crystalline anisotropy field, demagnetizing field $\mathbf{H}_d$, and DMI field $\mathbf{H}_{\text{DM}}$.

In the absence of energy source like an electric current, the LLG equation describes a dissipative system whose energy can only decrease[39,40]. Thus, solving LLG equation is an efficient way to find stable spin textures. In the present case, we apply periodic boundary conditions to eliminate the edge effects. We use the Mumax3 package[35] to numerically solve the LLG equation with mesh size of 1 nm × 1 nm × 0.4 nm for those skyrmions of $L > 5$ nm. For skyrmions of $L < 5$ nm, the mesh size is 0.1 nm × 0.1 nm × 0.4 nm. The number of stable states and their structures should not depend on the Gilbert damping constant, but spin dynamics is very sensitive to α. To speed up our simulations, we use a large α of 0.25 and 1. We consider only material parameters that support condensed skyrmion states. The skyrmion size L is obtained directly from numerical data or by fitting the simulated spin profile to $\Theta(x) =$ $2\arctan\left[\frac{\sinh(L/2w)}{\sinh(|x|/w)}\right]$ (the black stripes for $m_z \leq 0$) and $\Theta(x) = 2\arctan\left[\frac{\sinh(|x|/w)}{\sinh(L/2w)}\right]$ (white stripes for $m_z \geq 0$) with stripe width L and wall width w. Here $-L/2 \leq x \leq L/2$ and $x = 0$ is the centre of a stripe. It should be pointed out that the physics discussed here does not depend on the boundary conditions. However, different boundary conditions have different confinement potentials (or potential well depth) for stripe skyrmions, and can affect the maximal skyrmion number density below which a condensed skyrmion state is metastable.

Energy density of a film filled by stripes. Following similar assumptions as those in Ref. [19], we can compute the energy density of a system filled with stripes of width L that parallel to the y-axis and are periodically arranged along the x-axis. If Θ is the polar angle of spins and spin profile is $\Theta(x) = 2\arctan\left[\frac{\sinh((|x-nL|)/w)}{\sinh(L/2w)}\right] + n\pi$ with integer n and $x \in ((n-0.5)L, (n+0.5)L)$ as shown in Fig. 2a, the total energy of the film in the range of $y_1 < y < y_2$ and $x_1 < x < x_2$ is

$$E_{\text{total}} = d\int_{y_1}^{y_2}\int_{x_1}^{x_2} [A(\partial_x\Theta)^2 - D\partial_x\Theta + K\sin^2\Theta]\,\mathrm{d}x\mathrm{d}y.$$

$x_2 - x_1$ and $y_2 - y_1$ are much bigger than L, we need only to minimize energy density $E = E_{\text{total}}/[d(x_2-x_1)(y_2-y_1)]$. Then one has

$$E = \frac{1}{L}\int_{-L/2}^{L/2}\left[A\left(\frac{\partial\Theta}{\partial x}\right)^2 - D\frac{\partial\Theta}{\partial x} + K\sin^2\Theta\right]\mathrm{d}x. \tag{4}$$

In terms of $\epsilon = L/(2w)$, terms in E are,

$$E_{\text{ex}} = \int_{-L/2}^{L/2} A\left[\frac{\partial\Theta(x)}{\partial x}\right]^2 \mathrm{d}x$$
$$= \frac{A}{w^2}\int_{-L/2}^{L/2}\left[\frac{2\sinh(L/w)\cosh(x/w)}{\sinh^2(L/w) + \sinh^2(x/w)}\right]^2 \mathrm{d}x$$
$$= \frac{2A}{L}\int_{-1}^{1}\left[\frac{2\epsilon\sinh(\epsilon)\cosh(\epsilon x)}{\sinh^2(\epsilon) + \sinh^2(\epsilon x)}\right]^2 \mathrm{d}x,$$
$$= \frac{4A}{L}g_1(\epsilon)$$

$$E_{\text{DM}} = -D\int_{-L/2}^{L/2}\frac{\partial\Theta(x)}{\partial x}\mathrm{d}x$$
$$= -D\left[\Theta(L/2) - \Theta(-L/2)\right] = -\pi D,$$

$$E_{\text{an}} = \int_{-L/2}^{L/2} K\sin^2\Theta(x)\mathrm{d}x$$
$$= K\int_{-L/2}^{L/2}\left[\frac{2\sinh(L/2w)\sinh(x/w)}{\sinh^2(L/2w) + \sinh^2(x/w)}\right]^2 \mathrm{d}x$$
$$= \frac{K}{2}\int_{-1}^{1}\left[\frac{2\sinh(\epsilon)\sinh(\epsilon x)}{\sinh^2(\epsilon) + \sinh^2(\epsilon x)}\right]^2 L\,\mathrm{d}x$$
$$= KLg_2(\epsilon).$$

Add the three terms up, the energy density E is

$$E = \frac{4A}{L^2}g_1(\epsilon) - \frac{\pi D}{L} + Kg_2(\epsilon).$$

In terms of L, ϵ, $\xi = A/D$ and $\kappa = \pi^2 D^2/(16AK)$, we obtain Eq. (2),

$$E = \frac{4D}{\xi}\left[\frac{\xi^2}{L^2}g_1(\epsilon) - \frac{\pi\xi}{4L} + \frac{\pi^2}{64\kappa}g_2(\epsilon)\right].$$

The first and the third terms on the right-hand side are positive, thus

$$E \geq \frac{4D}{\xi}\left[\sqrt{\frac{4\pi^2\xi^2}{64L^2\kappa}g_1(\epsilon)g_2(\epsilon)} - \frac{\pi\xi}{4L}\right] = \frac{\pi D}{L}\left[\sqrt{\frac{g_1 g_2}{\kappa}} - 1\right].$$

To have negative E, κ must be larger than $\sqrt{g_1 g_2} \geq 1$.

Data availability
The data that support the plots within this paper and other findings of this study are available from the corresponding author on a reasonable request.

References
1. Skyrme, T. H. R. A unified field theory of mesons and baryons. *Nucl. Phys.* **31**, 556–569 (1962).
2. Mühlbauer, S. et al. Skyrmion lattice in a chiral magnet. *Science* **323**, 915–919 (2009).
3. Yu, X. Z. et al. Real-space observation of a two-dimensional skyrmion crystal. *Nature* **465**, 901–904 (2010).
4. Yu, X. Z. et al. Near room temperature formation of a skyrmion crystal in thin-films of the helimagnet FeGe. *Nat. Mater.* **10**, 106–109 (2011).
5. Heinze, S. et al. Spontaneous atomic-scale Magnetic skyrmion lattice in two dimensions. *Nat. Phys.* **7**, 713–718 (2011).
6. Romming, N. et al. Writing and deleting single magnetic skyrmions. *Science* **341**, 636–639 (2013).
7. Onose, Y., Okamura, Y., Seki, S., Ishiwata, S. & Tokura, Y. Observation of magnetic excitations of skyrmion crystal in a helimagnetic insulator Cu_2OSeO_3. *Phys. Rev. Lett.* **109**, 037603 (2012).
8. Bogdanov, A. N. & Rößler, U. K. Chiral symmetry breaking in magnetic thin films and multilayers. *Phys. Rev. Lett.* **87**, 037203 (2001).
9. Rößler, U. K., Bogdanov, A. N. & Pfleiderer, C. Spontaneous skyrmion ground states in magnetic metals. *Nature* **442**, 797–801 (2006).
10. Sampaio, J., Cros, V., Rohart, S., Thiaville, A. & Fert, A. Nucleation, stability and current-induced motion of isolated magnetic skyrmions in nanostructures. *Nat. Nanotechnol.* **8**, 839–844 (2013).
11. Li, J. et al. Tailoring the topology of an artificial magnetic skyrmion. *Nat. Commun.* **5**, 4704 (2014).
12. Back, C. et al. The 2020 skyrmionics roadmap. *J. Phys. D: Appl. Phys.* **53**, 363001 (2020).
13. Jiang, W. et al. Blowing magnetic skyrmion bubbles. *Science* **349**, 283–286 (2015).
14. Du, H. et al. Edge-mediated skyrmion chain and its collective dynamics in a confined geometry. *Nat. Commun.* **6**, 8504 (2015).
15. Yuan, H. Y. & Wang, X. R. Creation and Manipulation by Nano-Second Current Pulses. *Sci. Rep.* **6**, 22638 (2016).
16. Uchida, M., Onose, Y., Matsui, Y. & Tokura, Y. Real-Space Observation of Helical Spin Order. *Science* **311**, 359–361 (2006).
17. Han, J. H., Zang, J. D., Yang, Z. H., Park, J. H. & Nagaosa, N. Skyrmion lattice in a two-dimensional chiral magnet. *Phys. Rev. B* **82**, 094429 (2010).
18. Butenko, A. B., Leonov, A. A. & Rößler, U. K. Stabilization of skyrmion textures by uniaxial distortions in noncentrosymmetric cubic helimagnets. *Phys. Rev. B* **82**, 052403 (2010).
19. Rohart, S. & Thiaville, A. Skyrmion confinement in ultrathin film nanostructures in the presence of Dzyaloshinskii–Moriya interaction. *Phys. Rev. B* **88**, 184422 (2013).
20. Leonov, A. O. et al. The properties of isolated chiral skyrmions in thin magnetic films. *New J. Phys.* **18**, 065003 (2016).
21. Bogdanov, A. & Hubert, A. Thermodynamically stable magnetic vortex states in magnetic crystals. *J. Magn. Magn. Mater* **138**, 255–269 (1994).
22. Jiang, W. et al. Nanoscale magnetic skyrmions and target states in confined geometries. *Science* **349**, 283–286 (2015).
23. Yu, G. et al. Room-temperature skyrmions in an antiferromagnet-based heterostructure. *Nano. Lett.* **18**, 980–986 (2018).
24. Birch, M. T. et al. Real-space imaging of confined magnetic skyrmion tubes. *Nat. Commun.* **11**, 1–8 (2020).
25. He, M. et al. Realization of zero-field skyrmions with high-density via electromagnetic manipulation in Pt/Co/Ta multilayers. *Appl. Phys. Lett.* **111**, 202403 (2017).
26. Jena, J. et al. Evolution and competition between chiral spin textures in nanostripes with D2d symmetry. *Sci. Adv.* **6**, eabc0723 (2020).
27. Müller, J. et al. Magnetic skyrmions and skyrmion clusters in the helical phase of Cu_2OSeO_3. *Phys. Rev. Lett.* **119**, 137201 (2017).
28. Raju, M. et al. The evolution of skyrmions in Ir/Fe/Co/Pt multilayers and their topological Hall signature. *Nat. Commun.* **10**, 1–7 (2019).
29. Schoenherr, P. et al. Topological domain walls in helimagnets. *Nat. Phys.* **14**, 465–468 (2018).
30. Cortés-Ortuño, D. et al. Nanoscale magnetic skyrmions and target states in confined geometries. *Phys. Rev. B* **99**, 214408 (2019).
31. Ezawa, M. Compact merons and skyrmions in thin chiral magnetic films. *Phys. Rev. B* **83**, 100408 (2011).
32. Silva, R. L., Secchin, L. D., Moura-Melo, W. A., Pereira, A. R. & Stamps, R. L. Emergence of skyrmion lattices and bimerons in chiral magnetic thin films with nonmagnetic impurities. *Phys. Rev. B* **89**, 054434 (2014).
33. Nagaosa, N. & Tokura, Y. Topological properties and dynamics of magnetic skyrmions. *Nat. Nanotechnol.* **8**, 899 (2013).
34. Wang, X. S., Yuan, H. Y. & Wang, X. R. A theory on skyrmion size. *Commun. Phys.* **1**, 31 (2018).
35. Vansteenkiste, A. et al. The design and verification of MuMax3. *AIP Adv.* **4**, 107133 (2014).
36. Fert, A., Reyren, N. & Cros, V. Magnetic skyrmions: advances in physics and potential applications. *Nat. Rev. Mater.* **2**, 17031 (2017).
37. Zhang, X. et al. Skyrmion-electronics: writing, deleting, reading and processing magnetic skyrmions toward spintronic applications. *J. Phys.: Condens. Matter* **32**, 143001 (2020).
38. Sun, Z. Z. & Wang, X. R. Fast magnetization switching of Stoner particles: A nonlinear dynamics picture. *Phys. Rev. B* **71**, 174430 (2005).
39. Wang, X. R., Yan, P., Lu, J. & He, C. Magnetic field driven domain-wall propagation in magnetic nanowires. *Ann. Phys. (NY)* **324**, 1815–1820 (2009).
40. Wang, X. R., Yan, P. & Lu, J. High-field domain wall propagation velocity in magnetic nanowires. *Europhys. Lett.* **86**, 67001 (2009).

Author contributions
X.R.W. planned the project and wrote the manuscript. X.C.H. and H.T.W. performed theoretical and numerical simulations, and prepared the figures. All authors discussed the results and commented on the manuscript.

Competing interests
The authors declare no competing interests. X.R. Wang is an Editorial Board Member for Communications Physics, but was not involved in the editorial review of, or the decision to publish this article.

Additional information
Supplementary information The online version contains supplementary material available at https://doi.org/10.1038/s42005-021-00646-9.

Correspondence and requests for materials should be addressed to X.R.W.

Peer review information Communications Physics thanks the anonymous reviewers for their contribution to the peer review of this work. Peer reviewer reports are available

Reprints and permission information is available at http://www.nature.com/reprints

Publisher's note Springer Nature remains neutral with regard to jurisdictional claims in published maps and institutional affiliations.